

Infrared Active Phonons and Optical Band Gap in Multiferroic GdMnO₃ Studied by Infrared and UV-Visible Spectroscopy

S.H. BUKHARI AND J. AHMAD

Solid State Spectroscopy Laboratory, Department of Physics, Bahauddin Zakariya University, Multan 60800, Pakistan

(Received November 7, 2014; in final form December 9, 2015)

Optical properties of multiferroic GdMnO₃ synthesized by sol-gel method have been investigated by measuring the infrared reflectivity and UV-visible absorption spectra. The infrared reflectivity spectrum of polycrystalline GdMnO₃ in the frequency range 30–7500 cm⁻¹ at room temperature contains several phonon modes. The resonant frequency of observed infrared active phonon modes is found comparable with theoretically predicted results. Mean Born effective charges are calculated and discussed in view of the origin of ferroelectricity in GdMnO₃. Three strong absorption peaks observed in the UV-visible spectrum are attributed to the Mn (3d)-electron transitions. The optical band gap \approx 1.2 eV is estimated from UV-visible absorption spectrum using Tauc's relation. GdMnO₃ seems to behave like an indirect gap semiconductor.

DOI: [10.12693/APhysPolA.129.43](https://doi.org/10.12693/APhysPolA.129.43)

PACS: 63.20.-e, 78.20.-e, 72.20.-i, 73.20.Mf

1. Introduction

Revival of interest in rare earth doped orthorhombic perovskite RMnO₃ (R — rare earth) compounds stems from their potential technological applications and remarkable properties such as multiferrocity and colossal magnetoresistance [1, 2]. There has been an intensive search for new multiferroic materials, which exhibit magnetoelectric (ME) effect, ferroelectric (FE) and ferromagnetic (FM) order approximately. Such type of multiferroic properties have been observed in a number of oxide compounds including rare earth manganite RMnO₃ and RMn₂O₅ [3–5]. GdMnO₃ (GMO) is a multiferroic rare-earth manganite from the family of RMnO₃; where magnetic and ferroelectric orders coexist [4]. Moreover, GdMnO₃ undergoes a phase transition from paramagnetic to an incommensurate antiferromagnetic (ICAFM) order at $T_N \approx 42$ K and upon cooling, a second anomaly appears at $T_N \approx 22$ K which is associated with the transition from ICAFM into a canted antiferromagnetic (A-type AFM) ordering of the Mn³⁺ spin [6].

Previously, it was believed that ferroelectricity in ABO₃ compounds requires the off-centering of d^0 cation on the B-site along with magnetic ordering which requires unpaired spins [7]. However, now it is evident that origin of ferroelectricity in magnetic materials is possible with four mechanisms: magnetic ordering, lone-pair, charge ordering and geometric frustration. Recently, pyroelectric property and ferroelectricity in polycrystalline GdMnO₃ has been observed in terms of Gd–Mn spin interaction [8, 9]. However, contradictory results have been reported regarding the ferroelectric properties in GMO single crystal [9].

Infrared reflectivity spectroscopy is a helpful technique to elucidate the origin of ferroelectricity. Indeed, infrared reflectivity spectroscopy allows us to investigate for a possible soft phonon mode driven ferroelectric transition or to extract average Born effective charge through the so-

called longitudinal optical (LO)-transverse optical (TO) phonons splitting [10–12]. Pimenov et al. reported on the terahertz and far-infrared reflectance of GdMnO₃ single crystal and investigated electromagnons and phonons as a function of magnetic field and temperature [13, 14]. The electromagnons are strongly coupled to phonons and contribute to the static dielectric constant. Also, Ferreira et al. reported infrared reflectivity spectra of polycrystalline EuMnO₃ and GdMnO₃ obtained at various temperature where they discussed dielectric relaxation, phonon dielectric response, and the spin-phonon coupling phenomena [15]. It was also observed that the spectral signature of EuMnO₃ and GdMnO₃ is very approxilar and overall spectra do not change with temperature. Moreover, temperature dependent far-infrared reflectivity of polycrystalline NdMnO₃ have been investigated [16]. It was observed that no new phonon has been detected, so the number of modes remains unchanged in the whole low temperature range. Two main features are approxilar in the infrared reflectivity spectra of polycrystalline EuMnO₃, GdMnO₃ and NdMnO₃: no new phonon has been observed with changing temperature which indicates the static lattice distortion and the overall spectra signature is very approxilar which confirms that these compounds adopt the same crystal structure. On the other hand, optical conductivity and Born effective charges of these three polycrystalline compounds and phonon assignment of EuMnO₃ and GdMnO₃ have not been investigated yet, to the best of our knowledge.

In this paper, we report on the measurement of unpolarized reflectivity spectra of polycrystalline GdMnO₃ at room temperature. Phonon modes are assigned by comparing the theoretically predicted infrared active modes for orthorhombic RMnO₃. Born effective charges are calculated and discussed in view of understanding the multiferroic character of GMO. Optical band gap has been calculated from absorption spectrum.

2. Experimental

Polycrystalline sample of GdMnO_3 was prepared by sol-gel method. According to the formula GdMnO_3 stoichiometric amount of gadolinium nitrate and manganese nitrate were dissolved in distilled water with ratio $\text{Gd:Mn} = 1:1$. After it turned into a clean solution without any residues, citric acid was added in the molar ratio 1.5:1. Subsequently an appropriate amount of aqua ammonia solution was dissolved keeping the pH value to ≈ 7 . The resultant solution was continuously stirred by using a magnetic agitator and was evaporated by heating at 80°C until viscous gel was formed. Afterwards, the gel was ignited by increasing the temperature up to 200°C for 2 h and grounded into fine black powder. Finally, the obtained black precursor powder was sintered at 900°C for 6 h. Single phase character of the prepared sample have been checked using X-ray diffraction pattern. Room temperature infrared reflectivity has been measured using Fourier transform infrared spectrometer (Vertex 80v) at near-normal incidence mode. For the IR measurement, one of the surfaces of the disc shaped sample of diameter ≈ 13 mm was made smooth. The frequency range of $30\text{--}7500\text{ cm}^{-1}$ has been covered using KBR-DLaTGS and Mylar $6\ \mu\text{m}$ -DLaTGS beam splitter-detector combinations. The absorption spectra in the $200\text{--}1200\text{ nm}$ wavelength region has been obtained using UV-visible grating-type spectrometer.

3. Results and discussion

The X-ray diffraction pattern recorded on a powder of GMO using $\text{Cu } K_\alpha$ radiation at room temperature is shown in Fig. 1. All diffraction peaks have been indexed assuming orthorhombic structure with $Pbnm$ space group (JCPDS NO: 00-025-0337). Absence of unindexed peaks manifests the purity of phase of GMO. The lattice parameters computed are $a = 5.31\ \text{\AA}$, $b = 5.84\ \text{\AA}$ and $c = 7.43\ \text{\AA}$, which are consistent with theoretically predicted values [18].

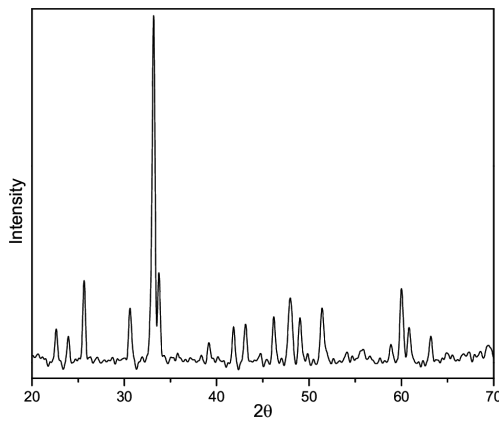


Fig. 1. XRD patterns of GdMnO_3 recorded at room temperature.

The reflectivity spectrum of GMO in the frequency range $30\text{--}800\text{ cm}^{-1}$ at room temperature is shown in

Fig. 2. The spectrum above 800 cm^{-1} was flat and structureless thus not shown here. Several phonons can be clearly seen as well as the reflectivity also remains finite at $\omega = 0$. Thus the spectrum resembles that of a typical semiconductor.

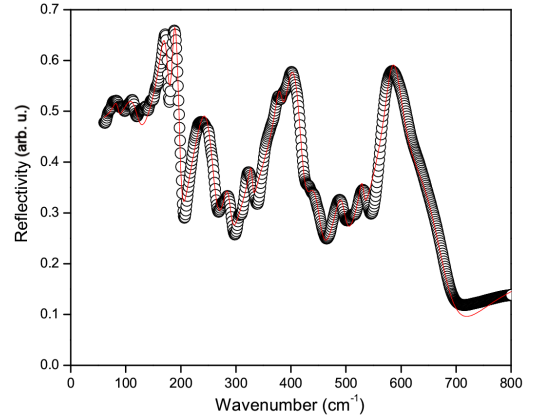


Fig. 2. The reflectivity spectrum of GdMnO_3 at room temperature. The raw data are plotted as open circles and solid line shows best fit of the Lorentz oscillators (see text).

To quantify optical phonons, we fitted the Lorentz oscillator model (LOM) to the reflectivity spectra. According to the LOM, the dielectric function $\epsilon(\omega)$ is defined as:

$$\epsilon(\omega) = \epsilon_\infty + \frac{\omega_{\text{TO},j}^2 S_j}{\omega_{\text{TO},j}^2 - \omega^2 - i\omega\gamma_j}, \quad (1)$$

$$R(\omega) = \left| \frac{1 - \sqrt{\epsilon(\omega)}}{1 + \sqrt{\epsilon(\omega)}} \right|^2, \quad (2)$$

where ϵ_∞ is the high-frequency dielectric constant, $\omega_{\text{TO}(j)}$, S_j and γ_j are the phonon frequency, oscillator strength and damping factor of j -th TO phonon, respectively.

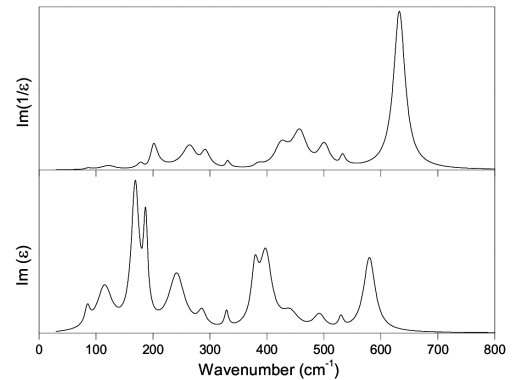


Fig. 3. The upper panel shows the loss function $\text{Im}(-1/\epsilon)$ and lower panel shows imaginary part $\text{Im}(\epsilon)$ of dielectric function, both calculated using the parameters obtained from the best fit of Lorentz oscillator model to the reflectivity spectrum of GMO.

In Fig. 3 the peak positions in the imaginary part of dielectric function $\text{Im}(\epsilon)$ and the loss function $\text{Im}(-1/\epsilon)$

correspond to TO and LO modes, respectively. Values obtained from phonon-fit parameters $\omega_{\text{TO},j}$, S_j , γ_j and longitudinal modes frequencies $\omega_{\text{LO},j}$ obtained from loss function $\text{Im}(-1/\epsilon)$ are given in Table I.

TABLE I

Phonon-fit parameters of reflectivity of GMO at room temperature.

ω_{TO}	[cm^{-1}]	ω_{LO}	γ_j	S_j
85		86	11	0.78
116		121	32	4.1
169		178	16.6	4.66
187		201	9	1.54
242		263	33.5	2.6
286		290	17	0.3
329		330	8	0.13
379		384	15	0.68
398		426	25.8	1.62
441		457	35	0.42
492		500	24	0.24
530		532	10	0.07
579		630	24.5	1.06

According to group theoretical analysis, there are 25 IR active phonon modes ($9B_{1u} + 7B_{2u} + 9B_{3u}$) in orthorhombic RMnO_3 structure (space group $Pnma$) [19]. These modes are classified into three phonon bands which corresponds to normal modes of the ideal cubic perovskite: external modes ($\omega < 290 \text{ cm}^{-1}$), bending mode at the intermediate range, and stretching modes ($\omega > 550 \text{ cm}^{-1}$). The low frequency external modes are due to the vibrations of R and MnO_6 , while the intermediate frequency range bending modes and the high frequency stretching modes mainly involve vibrations of oxygen octahedra [20]. Hence, the modes assignment will be made by comparing the phonon frequencies obtained from the fit with those found in lattice dynamics calculations [17, 24] as given in Table II. From Table II it is clear that some of the phonon modes obtained from the fit cannot be assigned unambiguously. For instance, the mode at 379 cm^{-1} could be associated with B_{2u} mode expected at 388 cm^{-1} or with B_{1u} mode at 367 cm^{-1} . Nevertheless, the ω_{TO} of the observed phonon modes are found in good agreement with those reported for the materials with approxilar crystal structure like polycrystalline NdMnO_3 [16], LaMnO_3 [17] and single crystal GdMnO_3 polarized along a -axis [13], as summarized in Table III.

As for the microscopic motion of the phonon modes is concerned, the phonon modes at 85, 116, 169, 187, and 242 cm^{-1} involve the motion of Gd atoms relative to MnO_6 octahedra. The Gd atoms, being heavier in the GdMnO_3 system, vibrate at low frequency. The mode associated to the vibration of Gd atoms is external mode. Moreover, the phonon modes at 286, 329, 379, and 398 cm^{-1} correspond to the complex motion of Mn atoms, relative to the displacement of oxygen atoms.

On the other hand, high frequencies modes at 441, 492, 530, and 579 cm^{-1} are attributed to the motion of oxygen atoms and in this frequency range, Gd and Mn atoms do not vibrate. These modes are usually called breathing modes as only oxygen atoms vibrate about their mean position relative to the Mn atoms.

TABLE II

Comparison of the best-fit resonant frequency (in cm^{-1}) of the phonon modes obtained for GMO with those of obtained by means of the lattice dynamics calculations as reported in Ref. [17] and Ref. [21].

This work	Ref. [17]	Ref. [21]
76 (B_{1u})	76 (B_{1u})	
85		86 (B_{3u})
		90 (B_{2u})
116	117 (B_{3u})	121 (B_{3u})
		135 (B_{1u})
		135 (B_{2u})
169		167 (B_{1u})
187		186 (B_{3u})
	191 (B_{2u})	
	194 (B_{1u})	
		202 (B_{3u})
		207 (B_{2u})
		225 (B_{3u})
	233 (B_{2u})	
	233 (B_{3u})	
242		244 (B_{1u})
		264 (B_{1u})
	273 (B_{1u})	
	276 (B_{3u})	
	283 (B_{2u})	
286	294 (B_{3u})	
		300 (B_{2u})
		306 (B_{3u})
		308 (B_{1u})
	318 (B_{1u})	
329	332 (B_{3u})	330 (B_{2u})
	334 (B_{1u})	
		367 (B_{1u})
379	388 (B_{2u})	
		394 (B_{1u})
398		399 (B_{3u})
	401 (B_{3u})	
	412 (B_{2u})	
	419 (B_{1u})	
	431 (B_{1u})	
441	443 (B_{3u})	
492	495 (B_{1u})	
		506 (B_{3u})
		516 (B_{2u})
530	521 (B_{3u})	
		562 (B_{2u})
579	577 (B_{1u})	579 (B_{1u})
	580 (B_{2u})	
	580 (B_{3u})	582 (B_{3u})
	625 (B_{2u})	

TABLE III

Comparison of ω_{TO} 's [cm^{-1}] of the phonon modes obtained for GMO with those reported for polycrystalline NdMnO_3 [16], LaMnO_3 [17] and single crystal GdMnO_3 [13].

Ref. [16]	Ref. [17]	Ref. [13]	This work
76	76		85
117	117	119	116
174	191	188	169
184	194		187
233	233	231	242
286	283	296	286
		308	
335	332	325	329
390	388		379
393	401	400	398
444	443	441	441
		460	
		475	
496	495	509	492
520	521	539	530
567	580	568	579
		641	

The phonons observed in the frequency between $\approx 270 \text{ cm}^{-1}$ and $\approx 550 \text{ cm}^{-1}$ are expected to give rise splitting of the bending mode of ideal perovskite structure. Similarly, frequencies exceeding $\approx 550 \text{ cm}^{-1}$ are assumed to originate orthorhombic symmetry of the stretching mode. Indeed, in the spectrum of GdMnO_3 , a number of modes have been observed above ≈ 270 , which reflects the strong orthorhombic distortions but we cannot classify any mode as purely bending or stretching mode. However, these modes greatly affect the changes of both Mn–O bond lengths and Mn–O–Mn bond angles.

For quantitative analysis of phonon contribution to the infrared spectrum of GMO, we have calculated optical conductivity $\sigma(\omega) = \omega\epsilon_2/4\pi$ spectrum as shown in Fig. 4. The $\sigma(0)$ is zero suggesting no contribution from free carriers at low frequency range. Moreover, the asymmetric shape of the phonon peaks is indicative of strong electron–phonon coupling in GMO.

The Born effective charges (Z^*) quantify the change in electron polarization response in a crystal upon ionic displacement. The Z^* reflect local dipole moment and play a central role in understanding physics of ferroelectric and even piezoelectric materials. Moreover, the Z^* directly influence the magnitude of the splitting of frequencies of the LO and the TO phonons. The Z^* is commonly related to the splitting of LO–TO modes, as

$$\frac{4\pi}{v_c} \sum_{k=1}^n \frac{Z_k^{*2}}{m_k} = 4\pi^2 \sum_{j=1}^N (\omega_{\text{LO}j}^2 - \omega_{\text{TO}j}^2), \quad (3)$$

where v_c is the unit cell volume, k is the sum over all atoms with mass m_k and j denotes the phonon mode. The condition of electric neutrality of a unit cell is $\sum_k Z_k^* = 0$. As our system is based on ternary com-

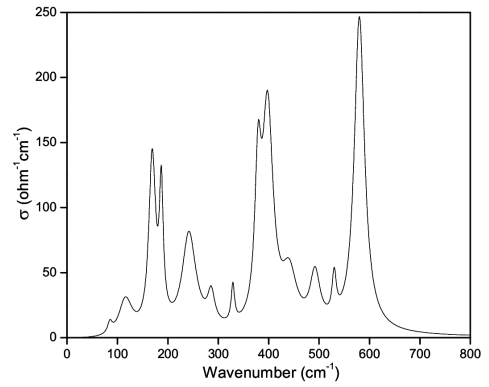


Fig. 4. Optical conductivity of GMO at room temperature.

pounds, the number of known exceeds the number of equation, this leads us to consider an additional hypothesis to calculate Z_k^* . As a result, one possibility is to consider the value of an effective charge of one atomic species equal to nominal ionic charge in order to determine the other two effective charges with a reasonably good accuracy. To get around this problem, we choose to set $Z_{\text{Mn}}^* = Z_{\text{Gd}}^*$ as a complementary equation, however, Gd and Mn ions have the same nominal ionic charge. In this way, we will be able to evaluate the mean Born effective charges since we cannot determine Z_{Mn}^* and Z_{Gd}^* separately. Therefore, we have calculated the Born effective charges by using the LO–TO splitting: $Z_{\text{Gd}/\text{Mn}}^* = 3.2$ and $Z_{\text{O}}^* = -2.1$. As polycrystalline sample has mixed *ab*-plane and *c* axis response, so the BEC have been calculated as an average over different optical response, however, it is believed that effective charges do not depend strongly on orientation [22]. The present Z^* values are quite close to those reported for other compounds of RMnO_3 such as DyMnO_3 [12], HoMnO_3 [23], LuMnO_3 [24], and YMnO_3 [25], as shown in Table IV. It is noteworthy that obtained values clearly deviate from their nominal values ($Z_{\text{Gd}/\text{Mn}} = 3$ and $Z_{\text{O}} = -2$) but small as compared with other ferroelectric materials such as BaTiO_3 , SrTiO_3 , WO_3 [26, 27].

TABLE IV

Mean Born effective charges of GMO deduces from LO–TO splitting in comparison with some other BEC's calculated for other compounds of RMnO_3 .

		Z^* (Mn or R)	Z^* (O)
This work	GdMnO_3	3.3	-2.2
$E \parallel c$	DyMnO_3	3.5	-2.3
	HoMnO_3	3.5	-2.3
	LuMnO_3	4.3	-2.9
	YMnO_3	4.7	-3.1
$E \parallel ab$	LuMnO_3	3.8	-2.5
	YMnO_3	3.7	-2.5

The UV-visible absorption spectrum of GdMnO_3 in the wavelength range 200–1100 nm is shown in Fig. 5.

The absorption spectrum of GMO is transformed from their diffuse reflectance spectrum according to the Kubelka–Munk theory [28]. Remarkably, the absorption cutoff wavelength in GMO sample is around 1100 nm which reflects that the present material can efficiently absorb light over a wide range of wavelength including whole visible spectrum (390–780 nm). Moreover, the strong absorption at about 455 nm indicate that GdMnO₃ sample prepared by this method could be a kind of photocatalytic material [29]. Also, three strong absorption peaks centered at 455 nm (2.7 eV), 505 nm (2.4 eV) and 612 nm (2.0 eV) indicated as arrows in Fig. 5 may be attributed to the Mn (3*d*)-electronic transitions in consistency with the reported behaviour [30].

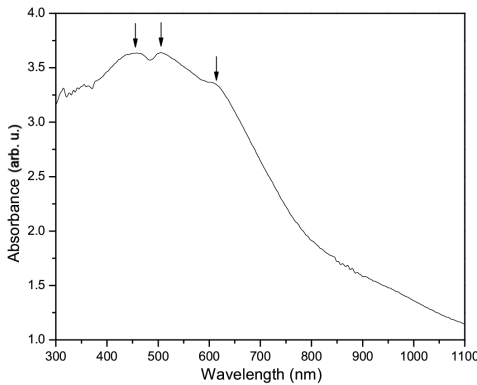


Fig. 5. The UV-visible absorption spectrum of GdMnO₃.

The optical bandgap energy of GMO is estimated by using the Tauc relation [31]:

$$\alpha hv = A(hv - E_g)^n, \quad (4)$$

where hv is the energy of incident photon, α is the absorption coefficient, A is a characteristic parameter, E_g is the optical band gap and n may be 1/2 or 2 for the direct or indirect transition, respectively. By using the Tauc relation, energy band gap can be estimated from the plot of $(\alpha hv)^{1/2}$ versus hv as shown in Fig. 6. The linear portion of the graph extrapolated to hv axis gives the value of energy band gap. The obtained indirect energy band gap of GMO is found to be ≈ 1.2 eV. The obtained value is quite approximate as observed for polycrystalline YMnO₃ [32] and YMn₂O₅ [33]. Recently, polycrystalline GdMnO₃ synthesized by sol-gel technique have been reported with the optical band gap of ≈ 2.9 eV [34], which is larger than our results as well as already reported by Wang et al. [30].

4. Conclusion

We have measured the reflectivity spectrum of polycrystalline GdMnO₃ at room temperature in the frequency range 30–7500 cm⁻¹. On comparison, an agreement was found between the experimental observed phonon modes and the two sets of calculated phonon frequencies together with the crystal symmetry. Moreover, a comparison of the other experimental observed

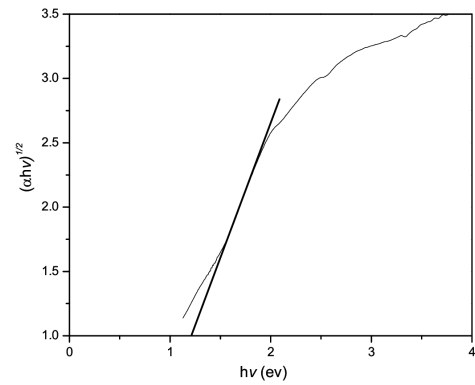


Fig. 6. The Tauc Plot of $(\alpha hv)^{1/2}$ versus hv , where the linear portion is extrapolated to the hv axis to obtain the energy band gap.

phonon modes of polycrystalline NdMnO₃ and LaMnO₃ are in good agreement with our observed phonon modes in GdMnO₃. On the contrary, infrared active phonon modes in single crystal GdMnO₃ are quite different from those observed in polycrystalline GdMnO₃. Moreover, from fit parameter we have calculated the mean Born effective charges such that $Z_{\text{Gd/Mn}}^* = 3.2$ and $Z_{\text{O}}^* = -2.1$. Remarkably, Born effective charges are unambiguously found to clearly deviate from their nominal valency, which provides a support towards ferroelectric polarization. In addition, we have calculated optical conductivity, and no contribution of free carriers have been observed. We have presented results of optical reflectivity and UV- visible absorption measurement on polycrystalline GdMnO₃ at room temperature. The absorption peaks centered at 2.0, 2.4 and 2.7 eV originates from the Mn (3*d*)-electronic transitions, while the optical band gap of about ≈ 1.2 eV is associated with the semiconducting behavior of GMO.

References

- [1] Y. Tokura, *J. Magn. Magn. Mater.* **310**, 1145 (2007).
- [2] N.A. Spaldin, M. Fiebig *Science* **309**, 391 (2005).
- [3] N. Hur, S. Park, P.A. Sharma, J.S. Ahn, S. Guha, S.W. Cheong, *Nature* **429**, 392 (2004).
- [4] T. Goto, T. Kimura, G. Lawes, A.P. Ramirez, Y. Tokura, *Phys. Rev. Lett.* **92**, 257201 (2004).
- [5] A.M. Shuvaev, A.A. Mukhin, A. Pimenov, *J. Phys. Condens. Matter* **23**, 113201 (2011).
- [6] J. Baier, D. Meier, K. Berggold, J. Herberger, A. Balbashov, J.A. Mydosh, T. Lorenz, *Phys. Rev. B* **73**, 100402(R) (2006).
- [7] N.A. Hill, *J. Phys. Chem. B* **104**, 6694 (2000).
- [8] L. Lin, L. Li, Z.B. Yan, Y.M. Tao, S. Dong, J.M. Liu, *Appl. Phys. A* **112**, 947 (2013).
- [9] X. Zang, Y.G. Zhao, Y.F. Cui, L.D. Ye, D.Y. Zhao, P.S. Li, J.W. Wang, M.H. Zhu, H.Y. Zhang, G.H. Rao, *Appl. Phys. Lett.* **104**, 062903 (2014).
- [10] J.F. Scott, *Phys. Rev. B* **4**, 1360 (1971).

- [11] X. Gonze, C. Lee, *Phys. Rev. B* **55**, 10355 (1997).
- [12] S. Jandl, S. Mansouri, J. Vermette, A.A. Mukhin, V.Yu. Ivanov, A. Balbashov, M. Orlita, *J. Phys. Condens. Matter* **25**, 475403 (2013).
- [13] A. Pimenov, T. Rudolf, F. Mayr, A. Loidl, A.A. Mukhain, A.M. Babashov, *Phys. Rev. B* **74**, 100403(R) (2006).
- [14] A. Pimenov, A.A. Mukhin, V.Yu. Ivanov, V.D. Travkin, A.M. Balbashov, A. Loidl, *Nature Phys.* **2**, 97 (2006).
- [15] W.S. Ferreira, J.A. Moreira, A. Almeida, M.R.C. Haves, J.P. Araújo, J.B. Oliveira, J.M. Machado Da Silva, M.A. Sá, T.M. Mendonça, P. Simeão Carvalho, J. Kreisel, J.L. Ribeiro, L.G. Vieira, P.B. Tavares, S. Mendonça, *Phys. Rev. B* **79**, 054303 (2009).
- [16] N.E. Massa, L. del Campo, D.D.S. Meneses, P. Echegut, M.J. Martínez-Lope, J.A. Alonso, *J. Phys. Condens. Matter* **25**, 395601 (2013).
- [17] I. Fedorov, J. Lorenzana, P. Dore, G. De Marzi, P. Maselli, P. Calvani, S.W. Cheong, S. Koval, P. Migoni, *Phys. Rev. B* **60**, 11875 (1999).
- [18] R. Ubic, G. Subodha, *J. Alloys Comp.* **488**, 374 (2010).
- [19] M.N. Iliev, M.V. Abrashev, H.G. Lee, V.N. Popov, Y.Y. Sun, C. Thomsen, R.L. Meng, C.W. Chu, *Phys. Rev. B* **57**, 2872 (1998).
- [20] M.D. Fontana, G. Metrat, J.L. Servoin, F. Gervais, *J. Phys. C Solid State Phys.* **17**, 483 (1984).
- [21] I.S. Smirnova, *Physica B* **262**, 247 (1999).
- [22] F. Gervais, *Solid State Commun.* **18**, 191 (1976).
- [23] J. Vermette, S. Jandl, M. Orlita, M.M. Gospodinov, *Phys. Rev. B* **85**, 134445 (2012).
- [24] A.B. Souchkov, J.R. Simpson, M. Quijada, H. Ishibashi, N. Hur, J.S. Ahn, S.W. Cheong, A.J. Millis, H.D. Drew, *Phys. Rev. Lett.* **91**, 027203 (2003).
- [25] M. Zaghrioui, V. Ta Phuoc, R.A. Souza, F. Gervais, *Phys. Rev. B* **78**, 184305 (2008).
- [26] P. Ghosez, P. Michenaud, J.X. Gonze, *Phys. Rev. B* **58**, 6224 (1998).
- [27] F. Detraux, P. Ghosez, X. Gonze, *Phys. Rev. B* **56**, 983 (1997).
- [28] P. Kubelka, F. Munk, *Z. Tech. Phys.* **12**, 593 (1931).
- [29] M.W. Kim, J.H. Jung, K.H. Kim, H.J. Lee, J. Yu, T.W. Noh, Y. Moritomo, *Phys. Rev. Lett.* **89**, 016403 (2002).
- [30] X.L. Wang, D. Li, T.Y. Cui, P. Kharel, W. Liu, Z.D. Zhang, *J. Appl. Phys.* **107**, 09B510 (2010).
- [31] J. Tauc, R. Grigorovici, A. Vancu, *Phys. Status Solidi* **37**, 627 (1966).
- [32] S.F. Wang, H. Yang, T. Xian, X.Q. Liu, *Catal. Commun.* **12**, 625 (2011).
- [33] H. Yang, S.F. Wang, T. Xian, Z.Q. Wei, W.J. Feng, *Mater. Lett.* **65**, 884 (2011).
- [34] P. Negi, G. Dixit, H.M. Agrawal, R.C. Srivastava, *J. Supercond. Nov. Magn.* **26**, 1611 (2013).